Macromolecules

Local Flips and Chain Motion in Polyethylene Crystallites: A Comparison of Melt-Crystallized Samples, Reactor Powders, and Nanocrystals

Ruth Bärenwald,[†] Sylvia Goerlitz,[‡] Reinhold Godehardt,[‡] Anna Osichow,[§] Qiong Tong,[§] Marina Krumova,[§] Stefan Mecking,[§] and Kay Saalwächter*,[†]

[†]Institut für Physik − NMR, Martin-Luther-Universität Halle-Wittenberg, Betty-Heimann-Str. 7, D-06120 Halle, Germany

[‡]Institut für Physik − Allgemeine Werkstoffwissenschaften, Martin-Luther-Universität Halle-Wittenberg, Von-Danckelmann-Platz 3, D-06120 Halle, Germany

[§]Chemische Materialwissenschaft, Fachbereich Chemie, Universität Konstanz, Universitätsstr. 10, D-78457 Konstanz, Germany

ABSTRACT: The crystallization and the mechanical properties of polyethylene, which is one of the most important commodity polymers, are influenced by the crystalline α-relaxation. This process originates from the diffusive chain transport through the crystallites as mediated by local 180° flips. Recent studies have stressed the relevance of the chain folding morphology on the chain diffusion, but its relation to the rate of jumps of the individual repeat units has not yet been addressed. In this study, we compare samples with very different morphology, including nanocrystals as a unique new model system, and use proton low-field and carbon-13 high-field solid-state NMR spectroscopy to determine the rate of local jumps and the large-scale crystalline−amorphous diffusion coefficient, respectively. We find that samples with tight folds (reactor powders and nanocrystals) display on average lower activation energies of the local jumps. Nanocrystals stand out in that they feature a significantly broader distribution of local jump rates, which we attribute to the location of stems in the finite nanocrystal. Our results for the crystalline−amorphous long-range diffusion are at partial variance with previous findings in that samples with tight folds do not generally exhibit the fastest diffusion, and we discuss the related ambiguities. Our data suggest that the higher chain mobility in the amorphous domain of melt-crystallized samples has an accelerating effect on intracrystalline chain dynamics at high temperatures but is accompanied by a more progressive slowdown at low temperatures due to cooperativity effects.
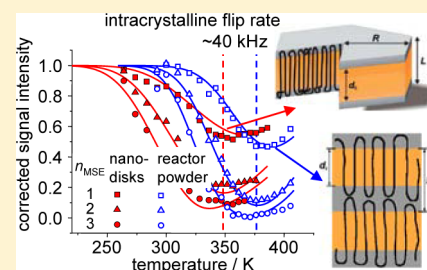
I. INTRODUCTION

Polyethylene (PE) is one of the most important commodity polymers, and its properties vary widely, depending on its specific microstructure and semicrystalline morphology. Linear PE exhibits diffusive chain motion of its all-trans chains through the crystallites and is thus classified as crystal-mobile.[1] This process is closely related to its crystallization behavior and crystallinity[2] and thus crucially influences many technologically relevant mechanical properties of the polymer, such as drawability[1] and creep.[3]

Early debates on the molecular origin of the chain translation[4] based upon conformational energy calculations considered a single type of a diffusing localized defect[5] or an extended 180° twisted region,[6] while more recent molecular dynamics simulations[7] have settled on a variety of defect structures that enable large-scale chain diffusion and conclude on a crystal-thickness independence. Yet, this stands in contrast to changes in the macroscopically detected mechanical crystalline α-relaxation,[2] which however only provides indirect information on the intracrystalline chain motion in PE.

Studying the morphology dependence of such local processes in order to truly understand their contribution to macroscopic properties requires well-defined samples, where single crystals grown from dilute solution[8,9] have long been the only and of course laborious option. Using such samples, for instance the process of lamellar doubling could be identified,[10] which is a special case of the lamellar thickening process[11] that is typical (and only possible) for crystal-mobile polymers.[1] A unique and much simpler model approach has recently emerged by Ni(II)-mediated catalytic polymerization of ethylene in dilute aqueous solution, which affords well-defined PE nanocrystals.[12−14] These disklike structures are very well-defined, with thickness and diameter in the 6−15 and 20−30 nm ranges, respectively, as controlled by equilibrium thermodynamics,[13,14] consisting of about 1−10 tightly folded chains oriented parallel to the disk normal. Here, we study, for the first time on the same sample, local and larger-scale chain dynamics in these nanocrystals and compare the results to other morphologies, i.e., ultrahigh molecular weight PE (UHMWPE) reactor powder[15] and various melt-crystallized samples. We characterize the samples with X-ray scattering and electron microscopy and use solid-state NMR as a microscopic probe of the dynamics.[16−18]
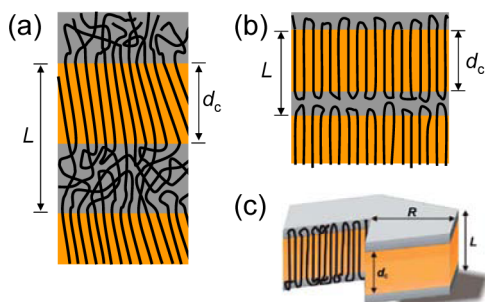
As noted, early work devoted to the experimental study of the intracrystalline dynamics relied on indirect observations by mechanical or dielectric spectroscopy.[2,6] Now, it is established that the local jump motion[19−21] as well as the large-scale chain diffusion[22−24] can best be studied on a molecular scale by different solid-state NMR methods. The important work of Hu, Boeffel, and Schmidt-Rohr employing a complicated dipolar ^{13}C-based experiment revealed that chain translation is indeed mediated by a 180° jump of a monomer,[19,20] which can of course effectively arise from the migration of a short-lived defect. This type of studies is rather limited in its scope due to the long experimental times and the need of a special doubly isotope-labeled sample.

Thus, more detailed insights into the influence of morphology on intracrystalline dynamics have so far only been taken from exchange experiments based upon ^{13}C longitudinal magnetization[22−24] characterizing the larger-scale chain diffusion. In particular, the findings of Yao et al.[23,24] were interesting, in that it was found that adjacent-reentry type solution-grown crystals exhibit much faster apparent chain diffusion than melt-crystallized counterparts with however the same activation energy. This was explained by a reduced entropic penalty related to the more constrained amorphous loops in the solution-grown crystals[25] and by introduction of a concept of an effective jump rate responsible for chain diffusion which should differ from the actual local jump rate.[23,24] These conclusions are, however, at variance with recent results from computer simulations of a polyethylene-like polymer,[26] where the intracrystalline chain diffusion was found to feature a broad distribution of correlation times, with the least mobile chains being those that exhibit tight folds. We have recently established a [1]H-based low-field method which enables direct access to the actual local jump rate without the need for special samples.[21] This puts us now into a position to scrutinize and refine these findings in two regards, i.e., studying nanocrystal samples of well-defined morphology and comparing these results with the local and larger-scale dynamics of various other samples.

II. MATERIALS AND METHODS

A. Samples. We compare three different PE sample types from different sources. The investigated morphologies are schematically shown in Figure 1. All relevant parameters of the samples are compiled in Table 1. Ideal PE nanocrystals[12,14] were prepared as described previously[27] via polymerization of ethylene with a Ni(II)-based catalyst in aqueous environment and subsequent removal of the solvent and the surfactant. The nanodisks (nd) have the form of truncated lozenges, each of them consisting of a 6−9 nm thick crystalline lamella embedded between two ∼1 nm thick amorphous layers containing the tight chain folds.[12,14]

The two samples differ only slightly; the PEnd1 have radii of $R \approx 12$ nm, and those of PEnd2 are of the same order but show a wider distribution in particle size. The overall thickness L (long period) and the crystalline thickness d_c were determined by small-angle X-ray scattering (SAXS) and cryo-transmission electron microscopy (TEM) as described previously.[12,14] The actual difference between PEnd1 and PEnd2 is that the former contains a few methyl branches per 1000 carbon atoms, whereas PEnd2 is perfectly linear. This is due to different catalysts used in their preparation. Overall, the degree of crystallinity of these nanocrystals is high due to an orderly deposition of the growing chain on the crystal during polymerization.[14]

The other samples were already part of our previous publication,[21] to which we refer the reader for details. A commercial melt-crystallized high-density PE (HDPEm) sample with a weight-averaged molecular weight $M_w \sim 349$ kg/mol and a polydispersity PD ~ 21 was provided by Basell Polyolefine GmbH. We further investigated two nascent UHMWPE reactor powder samples (PErp5000 and PErp750), where the number indicates the approximate M_w in kg/mol. More information on the preparation and the properties of the reactor powder samples can be taken from ref 15.

The PErp samples should exhibit a predominant adjacent-reentry structure (see Figure 1b) but were shown to feature a relatively disordered and complex overall morphology.[28] Packing small pieces of these samples into rotors for high-resolution ^{13}C NMR lead to the pressure-induced formation of a small amount of monoclinic phase,[29] which is readily apparent from the spectra and was removed by short annealing for 15 min at 358 K, well below the temperatures of melting (>400 K) and potential lamellar doubling (∼380 K). We further tested the influence of extended annealing for 2 days at 363 K, at which the morphology as seen in TEM did not change appreciably. For a direct comparison, we also prepared a melt-recrystallized sample (PErp5000m) after melting at 433 K for 7 h in a vacuum and slow cooling to room temperature within about 30 min. This sample, in analogy to HDPEm, should exhibit a disordered fold surface (Figure 1a). All experiments were performed above the lowest reported glass transition temperature of the mobile amorphous regions in PE, $T_g \approx 150$ K,[30] below which the chains in the crystallites are no longer mobile.[1]

B. Structural Characterization. *TEM.* Transmission electron microscopy was used to determine the long period L and the crystalline thickness d_c of the HDPE and PErp samples.[31,32] Images were taken on a JEM 2010 instrument from ca. 80 nm thick slices stained with RuO_4. Amorphous regions and in particular the interfaces between crystalline lamellae and the adjacent amorphous material of the ultrathin sections are predominantly stained by the RuO_4. The sample images shown in Figure 2 demonstrate how the semicrystalline morphology is reflected in regions where many lamellae are oriented in nearly edge-on position. The ImageJ software was used to determine about 700 distances for every sample, and roughly estimated mean values for the long period, the crystalline thickness, and the resulting linear crystallinity are given in Table 1. Figure 2 demonstrates that the lamellar structure is much better visible in the melt-crystallized samples, while the reactor powders exhibit a rather fragmented structure, in agreement with the literature.[28] Annealing (15 min at 358 K vs 2 days at 363 K) did not have an appreciable effect on the morphology.

WAXS. Wide-angle X-ray scattering was employed to characterize the temperature-dependent crystalline lattice spacings and possible differences between the samples, using the Bragg equation based upon the known assignments.[33] The experiments were performed on a Bruker AXS Advance diffractometer using the Cu Kα line at 1.541 Å. The samples were measured as dried powders in an angle range 10° < 2θ < 80°. The lattice parameters a and b are plotted for two different temperatures in Figure 3. The lattice parameter c of the orthorhombic unit cell along the all-trans chain direction was the same at 303 and 373 K for all samples (2.546 ± 0.003 Å). It is seen that the thermal

Figure 1. Schematic morphologies of the investigated samples: (a) melt-crystallized PE with switchboard-like fold surface, (b) PE reactor powder with prevailing adjacent-reentry structure, and (c) ideal PE nanocrystals. L and d_c are the long period and the crystallite thickness, respectively.

Table 1. Properties of the PE Samples[a]

	M_w/kg/mol	PD	crystallinity	L/nm	d_c/nm	T_m/K
HDPEm	349	21.4	66% (TEM)	14 (TEM)	9 (TEM)	405
			59% (DSC)			
			60% (NMR)			
PErp5000m	5000	3	45% (NMR)	—[b]	17 (TEM)	412
PErp5000	5000	3	75% (NMR)			418
			66% (TEM)	11 (TEM)	7 (TEM)	
annealed (2 days, 363 K)			66% (TEM)	12 (TEM)	8 (TEM)	
PErp750	750	1.8	70% (NMR)			417
PEnd1[12]	200	2	70% (SAXS)	9 (SAXS)	6.3 (SAXS)	403
			80% (NMR)			
PEnd2[14]	588	1.4	80% (SAXS)	10.9 (SAXS)	8.8 (SAXS)	
			85% (NMR)			

[a]The crystallinities refer to ambient temperature, and their calculation from structural data (TEM: this work; SAXS: refs 12 and 14) assumes a simple lamellar arrangement. The melting points T_m were determined by differential scanning calorimetry at 20 K/min heating rate. [b]Insufficient number of well-stacked lamellae.
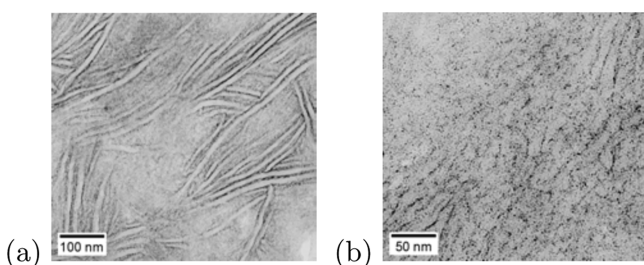

(a) 100 nm   (b) 50 nm

Figure 2. TEM images of the (a) HDPEm and (b) PErp5000 samples. The latter was annealed for 15 min at 358 K.
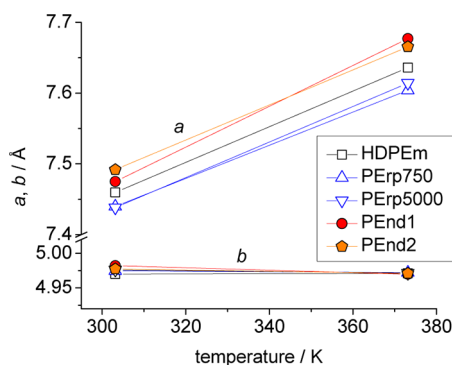

Figure 3. Lattice parameters a and b evaluated from WAXS peak positions for all samples as a function of temperature.

expansion affects mainly the a direction and that the nanodisk samples exhibit a slightly expanded unit cell as compared to the other samples.

Crystallinities. The crystallinity values determined with different methods as listed in Table 1 differ somewhat for each given type of sample, yet the ∼10% variation is well within the expected range considering the methodological differences and the approximations involved. A more detailed discussion for a part of the samples was published in ref 21, where the NMR values (see below) were discussed as a function of temperature. The trends observed for the new samples PErp5000m and PEnd1/2 studied herein matched the previous ones in that the melt-crystallized samples (HDPEm and PRrp5000m) exhibit a weak monotonic decrease by around 5% up to around 380 K, above which a stronger partial melting process sets in. The crystallinities of the PErp samples are nearly constant up to around 360 K, above which they increase by 5−10%, which can be explained by a lamellar thickening process. The crystallinities of the PEnd samples are nearly constant up to around 380 K, above which a reorganization process[14] and partial melting set in. We thus avoid this

temperature range but note that even below 370 K the PEnd samples, being ideal adjacent-reentry-type nanocrystals with thermodynamically controlled shape, exhibit lamellar thickening upon annealing, which means that the dimensions given in Table 1 can increase by about 50%.[13,14]
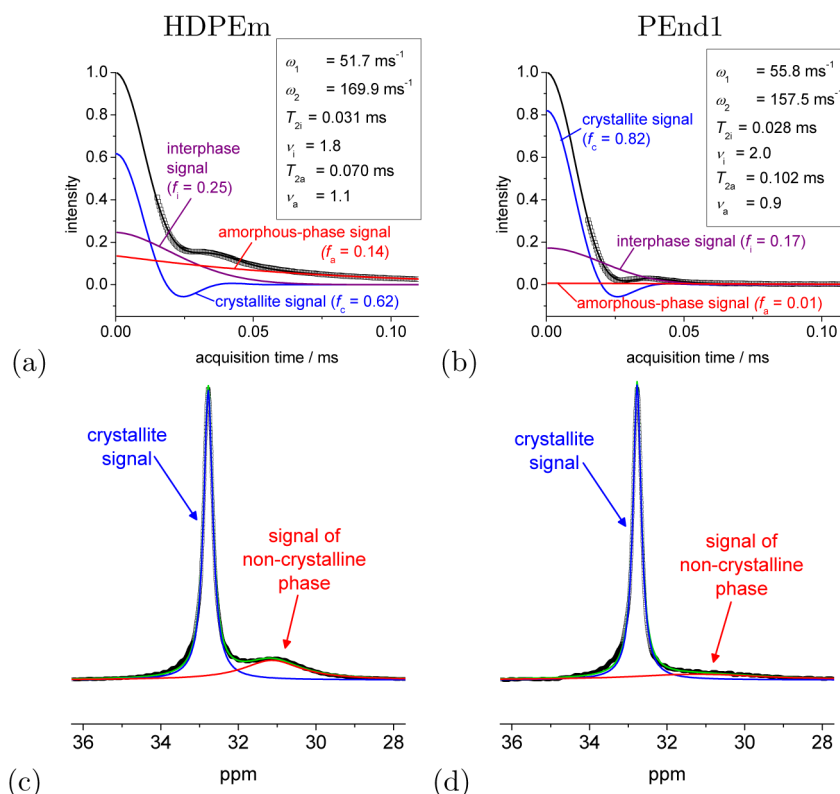
C. Solid-State NMR Spectroscopy. *¹H Low-Field NMR.* A Bruker minispec mq20 spectrometer with a static magnetic field of 0.5 T and a ¹H Larmor frequency of 19.95 MHz, equipped with a wide-temperature-range static probe, was used for the determination and investigation of the different (crystalline, amorphous, and intermediate rigid-amorphous) phase fractions of the PE samples in a range between 240 and 400 K. The method is based upon the simple detection of the free-induction decay (FID) after application of a 90° pulse (∼1.6 μs length), using a recycle delay of 2−5 s between individual scans to ensure quantitative detection of the full relaxed sample magnetization. The latter was set based upon saturation-recovery experiments to estimate the $T_1(^1H)$. In order to confirm the full shape of the FID at the lowest temperatures, we employed a mixed[34] magic-sandwich echo (MSE)[35] to overcome the receiver dead time of 15 μs. Since the echo is deteriorated and is changing its shape at higher temperatures and longer echo delays due to the intracrystalline dynamics (see below), we stabilized the fits by determining and fixing the intensity at zero acquisition time. This is easily possible by measuring the melt response at high temperature and using the $1/T$ Curie law to determine the intensity at a given lower temperature.

A proton FID in a rigid solid decays quickly (i.e., the spectral line is wide) due to the network of multiple strong distance-dependent dipole−dipole couplings between the spins. The dipole−dipole couplings are also orientation dependent, which means that molecular rotational motion on a time scale faster than the inverse rigid-limit spectral broadening (i.e., 20 μs or lower) leads to a reduction of the average dipolar spectral broadening and thus to a lengthening of the FID. In PE, we can distinguish three components on the basis of their different (nonexponential) T_2 relaxation behavior, in line with previous studies.[21,36,37] The first 200 μs of the FID were fitted to

$$\frac{I_{FID}(t)}{I_{FID}(0)} = f_c e^{(-1/2)(\omega_1 t)^2} \frac{\sin \omega_2 t}{\omega_2 t} + f_i e^{-(t/T_{2i}^*)^{\nu_i}} + f_a e^{-(t/T_{2a}^*)^{\nu_a}} \quad (1)$$

For details on the data acquisition and analysis procedures we refer to our previous work,[21] but note that the fits are quite stable due to the oscillatory feature of the so-called Abragam function (first term of the right-hand side of eq 1). The crystalline amplitude f_c as the main quantity of interest is thus determined rather reliably. Figure 4a,b shows FIDs for two different samples and their decomposition, and the indicated component fractions were used as NMR estimates for the crystallinity as given in Table 1. Notably, the nanodisk samples (as well as the reactor powders) exhibit virtually no mobile amorphous but

HDPEm

ω_1 = 51.7 ms^{-1}
ω_2 = 169.9 ms^{-1}
T_{2i} = 0.031 ms
ν_i = 1.8
T_{2a} = 0.070 ms
ν_a = 1.1

interphase signal (f_i = 0.25)

amorphous-phase signal (f_a = 0.14)

crystallite signal (f_c = 0.62)

(a)

PEnd1

ω_1 = 55.8 ms^{-1}
ω_2 = 157.5 ms^{-1}
T_{2i} = 0.028 ms
ν_i = 2.0
T_{2a} = 0.102 ms
ν_a = 0.9

crystallite signal (f_c = 0.82)

interphase signal (f_i = 0.17)

amorphous-phase signal (f_a = 0.01)

(b)

crystallite signal

signal of non-crystalline phase

(c)

crystallite signal

signal of non-crystalline phase

(d)

Figure 4. Low- and high-field NMR data: low-field FIDs of (a) HDPEm and (b) PEnd1 taken at about 308 and 400 K, respectively, along with component decompositions on the basis of eq 1, and (c, d) high-field ^{13}C CP MAS spectra of the respective same samples taken at about 300 K and fits of the crystalline and amorphous components using two Lorentzians.

only the more constrained but certainly not fully immobilized "rigid-amorphous" interphase,[38−40] in line with their tightly folded structure.[14]

Local chain flips in the crystallites are qualitatively detected through their time-dependent effect on the effective ^{1}H−^{1}H dipole−dipole coupling,[41,42] measured in terms of the second moment of the ^{1}H spectral line shape

$$M_2 = \omega_1{}^2 + \frac{1}{3}\omega_2{}^2 \tag{2}$$

which is calculated from the parameters ω_1 and ω_2 from the FID fitting, eq 1. The effect is subtle, as a 180° chain flip leaves the main dipole−dipole interactions of the protons within a given chain invariant, while only the weaker secondary couplings to neighboring chains are averaged out by the motion.

A novel and more quantitative assessment yields the average flip correlation time $\tau_c(T)$ and, in combination with temperature variation, the activation parameters and the logarithmic width of the τ_c distribution σ (in units of decades). It is based upon a detailed analysis of the signal decay under the mentioned MSE pulse sequence $I_{MSE}(t_{seq})$, where the sequence (full echo) time $t_{seq} = n_{MSE}t_c$ is given in multiples n_{MSE} of a cycle time $t_c \approx 88$ μs. The analysis relies upon the Anderson−Weiss (A−W) theory,[43] which yields the signal decay function[21,44]

$$I_{MSE}(t_{seq}, \Delta M_2^{dyn}, \tau_c) = \exp\left[-\Delta M_2^{dyn}\tau_c{}^2\left(e^{-t_{seq}/\tau_c} - 3e^{-5t_{seq}/6\tau_c}\right.\right.$$
$$\left.\left.+\frac{9}{4}e^{-2t_{seq}/3\tau_c}+3e^{-t_{seq}/6\tau_c} + \frac{t_{seq}}{2\tau_c} - \frac{13}{4}\right)\right] \tag{3}$$

that depends on the τ_c of the assumed two-site jump motion and on the associated decay amplitude ΔM_2^{dyn} of M_2 (this implies a—probably very good—assumption of time scale separation from additional fast small-angle librations). ΔM_2^{dyn} can be estimated from our data, and it is

noted that the analysis results are only weakly dependent on its absolute value. This special type of T_2 decay is thus sensitive to the time scale of changes in $M_2(t)$ in the range of μs to ms[44,45] due to the time and thus temperature dependence of M_2 imparted by the variable interchain couplings.

The signal decay under the MSE is nonexponential and is additionally affected by an M_2-dependent higher-order dipolar dephasing due to corrections of its average Hamiltonian arising mainly from the finite cycle time of the pulse sequence, which gives an extra Gaussian-shaped contribution characterized by an apparent decay time $T_{2,app}^{dd}$. This feature of the MSE has opened a popular field of applications as a "dipolar filter" used to suppress strongly dipolar-coupled sample fractions in the presence of weakly coupled, more mobile parts.[46] $T_{2,app}^{dd}$ displays a monotonic negative correlation with M_2 (which has not been explored in much detail yet), and we have used an empirical linear relation to correct the experimental I_{MSE} decay. It is noted that $T_{2,app}^{dd}$ should not be confused with the apparent signal decay time of the FID often referred to as T_2^* (which was unfortunately the case in our ref 21). The former is in fact 1−2 decades larger than the latter, as the higher-order dephasing effect relatively weak.

The exact procedure to obtain and then analyze the crystallite-specific $I_{MSE,c}^{corr}(t_{seq})$ decay, extracted from the full detected signal by way of fitting to eq 1, is described in detail in ref 21. The data could only be fitted well when a log-normal distribution of correlation times, $p(\tau_c, \mu, \sigma) = [(2\pi)^{1/2}\sigma\tau_c]^{-1}e^{-(\ln\tau_c-\mu)^2/2\sigma^2}$, was considered. The decadic full width at half-maximum of this distribution is $\sigma2(2\ln 2)^{1/2}/\ln 10 \approx \sigma$. The final fit for I_{MSE} was realized by on-the-fly numerical τ_c integration of eq 3 multiplied by $p(\tau_c, \mu, \sigma)$, and the average correlation time was obtained from the two fitted parameters as $\langle\tau_c\rangle = \exp(\mu + \sigma^2/2)$.

^{13}C High-Resolution Solid-State NMR. ^{13}C cross-polarization (CP) magic-angle spinning (MAS) spectra were acquired on a Bruker Avance III instrument with 400 MHz ^{1}H Larmor frequency using a Bruker 4 mm MAS WVT double-resonance probe head at 5 kHz

spinning frequency, relying on a flow of heated air for temperature regulation with an accuracy of about ±2 K. Typical 90° pulse lengths were 3 and 3.2 μs for ^{1}H and ^{13}C, respectively. [13]C spectra were usually taken with a 5 s recycle delay using CP, with 0.5 ms contact time using spin-lock nutation frequencies of 83 kHz and 71.5 kHz for ^{13}C and ^{1}H, respectively. SPINAL64[47] was used for ^{1}H dipolar decoupling at a nutation frequency of 83 kHz. The crystalline and amorphous regions of PE at 33 and around 31 ppm, respectively, can readily be distinguished in the spectra, based upon packing effects and the conformational mixture in the amorphous phase and the γ gauche effect.[48,49]

Sample spectra and deconvolutions using two Lorentzians (which provided the best minimal model) are shown in Figure 4c,d, and we note that they are not quantitative.[48] At higher temperatures, in particular for the melt-crystallized samples with their larger amorphous fraction, it was possible and necessary to introduce a third Lorentzian centered around 32 ppm accounting for a separate rigid-amorphous interphase fraction. Note that the virtual absence of this third component at lower temperatures does not imply that an interphase is not present and could not be identified with more advanced spectral editing techniques. The main goal of our fits was to obtain a reliable measure (amplitude, width, and integral) of the crystallite signal, the accuracy of which is estimated to about 5%.

Fast Bond Librations and Rotations. We have applied the well-known DIPSHIFT technique[50] to quantify the strength of the [13]C−[1]H heteronuclear dipole−dipole couplings (D_{CH}) at different temperatures. In comparison with the expected static-limit value $D_{CH,stat}/2\pi \approx$ 21 kHz, a potentially reduced D_{CH} reflects the amplitude of fast orientation fluctuations of the CH bonds in the CH$_2$ group with correlation times significantly below the inverse $D_{CH,stat}$, i.e., 10 μs or lower.[51] As opposed to the ^{1}H case discussed above, the influence of interchain couplings to remote protons is much weaker; the experiment thus provides rather local information. DIPSHIFT modulation curves, with the modulation time t_1 varying between 0 and the rotor period T_{rot}, were acquired for the crystalline and amorphous resonance positions using the pulse sequences described in previous publications[52,53] using an initial CP and Lee−Goldburg homodecoupling at an effective nutation frequency of 85 kHz (absolute nutation frequency of 62.5 kHz at 49.1 kHz offset).

Chain diffusion through the crystallites was studied by monitoring the exchange of ^{13}C longitudinal magnetization between the crystalline and amorphous regions,[22−24] making use of the fact that the T_1 relaxation time of amorphous carbons is short (<1 s), while it is longer than 200 s for the crystalline regions.[54] Thus, any experiment suitable to measure the T_1 relaxation time of the crystalline signal can be used to extract the desired information, as the apparent T_1 process is dominated by the motion into the amorphous domain, where T_1 is short. We chose to use Torchia's experiment,[55] which monitors the decay of z magnetization created by a short CP (50 μs, emphasizing the crystalline signal) during a z filter duration of variable length τ. The experiment has the advantage of providing a signal decay function with a well-defined limiting value of zero intensity and was used for the same purpose before by Yao et al.[23,24] A critical concept of this experimental concept is found in ref 22 and taken up below. None of the previous references[22−24] makes any explicit statement on the way how the crystallite signal was evaluated, so we compared the amplitude and the integral of the Lorentzian fitted to the crystalline component as plotted vs $\sqrt{\tau}$. In this representation, a linear decay indicates diffusive behavior, and the differences found for the two observables are discussed below.

III. RESULTS

We now first present the ^{1}H low-field NMR results characterizing the local flips in the PE crystallites, then discuss the [13]C−[1]H DIPSHIFT data reflecting fast bond librations in order to back up some of the drawn conclusions, and finally address ^{13}C-based chain diffusion coefficients, which we compare with chain diffusion coefficients derived from the ^{1}H data.

A. Local Flips As Characterized by ^{1}H Low-Field NMR.

Figure 5 compiles the low-field NMR data that qualitatively reflect the intracrystalline chain flip motion. Figure 5a shows the crystallite-specific second moment M_2 of the ^{1}H line shape and provides a good overview of the differences and commonalities among the different samples. Some of these results have been published previously;[21] new are the data from samples PErp5000m, PEnd1, and PEnd2.

The increasingly strong decrease of M_2 with rising temperature reflects the influence of the jump motion on interchain dipole−dipole couplings, as observed more than five decades ago by Olf and Peterlin.[41] In fact, the data for HDPEm and the two reactor powders, in particular the onset temperatures of the fast decay at around 360 K, are in almost quantitative agreement with their data. Note that the absolute values of M_2 depend sensitively on the choice of zero acquisition time, which for our minispec with its nonideal 90° pulses has an uncertainty in the 1−2 μs range, amounting to an absolute-value uncertainty of M_2 of around 30%. Further, the rather weak decay in the temperature range below 360 K is caused by small-amplitude chain oscillations (vibrations and phonons) and lattice expansion, leading to a slight decrease of the dipolar coupling strength due to some preaveraging and increasing mean proton distances, respectively.[41,42]

All data just reach a high-temperature plateau which characterizes the fast-limit averaged M_2 value for quickly flipping chains.[42] This defines a ΔM_2^{dyn} characterizing the overall drop in M_2. While M_2 has a specific temperature

(a)

(b)
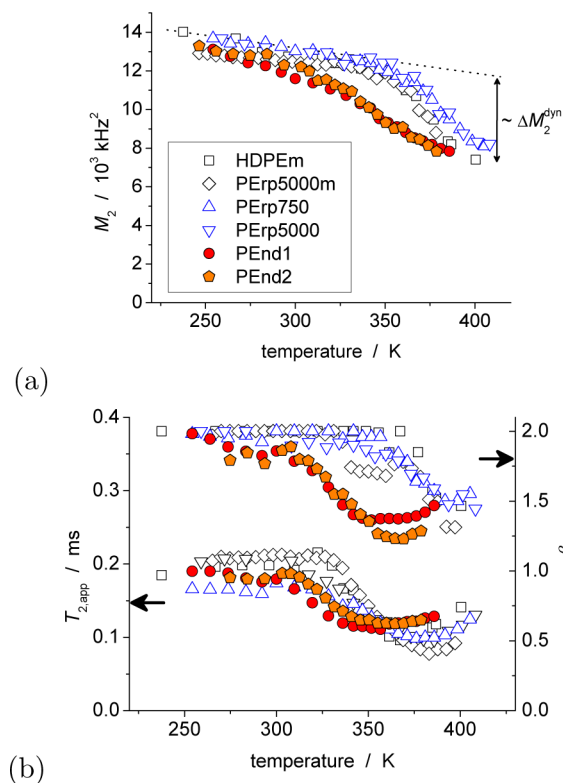
Figure 5. Low field NMR data reflecting intracrystalline chain flips: Temperature dependence of (a) the second moment of the crystallite line shape M_2 as calculated from eq 2 and (b) the fitting parameters $T_{2,app}$ (left y scale) and β (right y scale) to the MSE intensity decay given by eq 4. In (a), ΔM_2^{dyn} denotes the decay amplitude due to chain flips (see text).

Table 2. Results from the Fits to ^{1}H Low-Field and ^{13}C$-^1$H High-Field NMR Data Characterizing the Motions in PE Crystallites

	local flip process				chain diffusion
	$\Delta M_2^{\mathrm{dyn}}$/kHz^2	σ	$\log[\tau_{c,0}]$/s	E_a/kJ mol^{-1}	E_a^{diff}/kJ mol^{-1}
HDPEm	5720 ± 970	1.13 ± 0.45	−20.4 ± 2.6	114 ± 20	43.4 ± 1.2
PErp5000m	8200 ± 1300	1.15 ± 0.37	−20.3 ± 0.70	116 ± 6	65.5 ± 2.0
PErp5000	7800 ± 1400	2.02 ± 0.45	−13.7 ± 2.3	75 ± 11	64.0 ± 3.5
					66.4 ± 2.0^a
PErp750	5900 ± 1200	1.41 ± 0.38	−14.8 ± 1.6	77 ± 8	61.7 ± 2.1
PEnd1	5650 ± 480	2.85 ± 0.34	−11.1 ± 1.8	60 ± 11	30.6 ± 1.0
PEnd2	5750 ± 560	2.87 ± 0.23	−14.8 ± 4.4	87 ± 27	

^{a}Annealed (2 days, 363 K).

dependence, we assume $\Delta M_2^{\mathrm{dyn}}$ to be temperature-independent. Its value can be read off qualitatively and is found to be in qualitative agreement with the values taken from our model fits (see below and Table 2).

The most important qualitative observation is the initially quicker decay of the PEnd samples and a smeared and earlier onset of the jump-related decay. Initially, we assumed that the stronger decay below 360 K could be due to differences in the thermal expansion coefficients of the lattice parameters (leading to increase proton−proton distances) and/or some additional local fast-limit bond librations that may be possible in a slightly expanded crystal. Tight chain folds in the amorphous region, exerting a lateral stress, have in fact been made responsible for small changes in lattice spacing.[56−58] However, the WAXS data in Figure 3 prove that the lattice dimensions vary only weakly among the samples and that the linear expansion coefficients (slopes in that plot) are nearly equal. Notably, however, the PEnd samples do show a slightly expanded lattice in the *a* directions as compared to the other samples. This is again indicative of the model-type adjacent-reentry structure of the nanodisk samples. Thus, the WAXS observations, together with the ^{13}C$-^1$H DIPSHIFT data addressed in the next section, suggest that the quicker decay of the M_2 for the PEnd samples is due to different intracrystalline chain-flip dynamics.

The differences between the samples are even more clearly apparent in the parameters taken from the more quantitative decay of the crystallite-specific MSE intensities, which can be phenomenologically fitted to

$$\frac{I_{\mathrm{MSE,c}}(t_{\mathrm{seq}})}{I_{\mathrm{MSE,c}}(0)} = \exp\{-(t_{\mathrm{seq}}/T_{2,\mathrm{app}})^\beta\} \qquad (4)$$

Sample data are shown in ref 21. The MSE refocuses all dipole−dipole interactions to first order; thus, the intrinsically nonexponential decay directly reflects intermediate (μs to ms scale) motions, with the apparent refocused $T_{2,\mathrm{app}}$ going through a minimum when the flip process has a correlation time that roughly corresponds to the inverse of the dipole−dipole interaction.[21,44] In Figure 5b, we see the trends observed for $T_{2,\mathrm{app}}$ and the nonexponentiality parameter β to be consistently shifted to lower temperatures, indicating again faster chain-flip dynamics for the PEnd samples. In addition, visible changes in $T_{2,\mathrm{app}}$ set in already at lower temperatures, and the associated $T_{2,\mathrm{app}}$ minima are higher and broader, which indicates a broader distribution of correlation times.

A quantitative assessment of the observed $T_{2,\mathrm{app}}$ decays is possible by joint fitting of decay data taken at various temperatures after correction for the Gaussian-shaped low-temperature contribution to $T_{2,\mathrm{app}}$ (termed $T_{2,\mathrm{app}}^{\mathrm{dd}}$), which is

related to higher-order dipolar-dephasing Hamiltonian corrections to the MSE sequence (see the Materials and Methods section as well as ref 21). Sample data are shown in Figure 6a, where we again notice a shift of the relaxation time minimum (minimum of the intensity decayed in the given time) to lower temperatures for the PEnd1 sample and also its somewhat higher value, which arises from more pronounced dynamic inhomogeneity. The location of the minimum is again a rough indicator of the temperature at which the average correlation time of motion is of the order of the inverse coupling, with an additional shift related to the sequence length.[45]

For quantitative stable fitting, we simultaneously analyzed data taken for the three shortest values of $t_{\mathrm{seq}} = n_{\mathrm{MSE}}t_c$ (considering a minimum 88 μs cycle time t_c of the MSE) over the whole investigated temperature range by

(a)

(b)
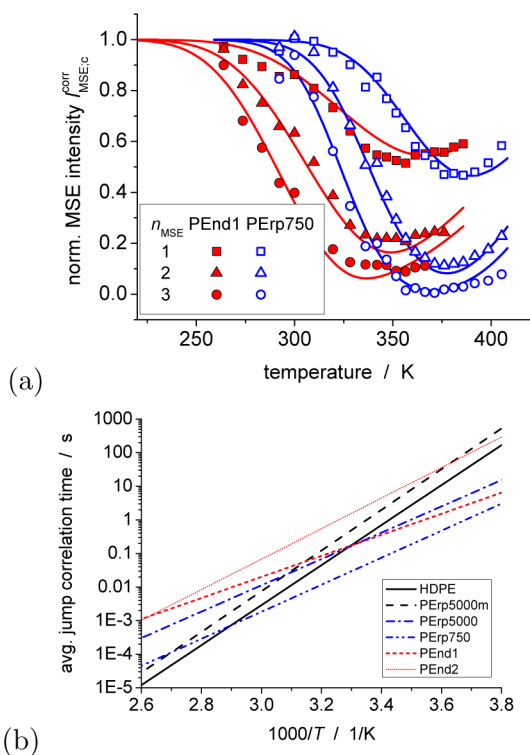
Figure 6. (a) Decay of the crystallite-specific, corrected MSE intensities $I_{\mathrm{MSE,c}}^{\mathrm{corr}}(t_{\mathrm{seq}})$ at fixed sequence times $t_{\mathrm{seq}} = n_{\mathrm{MSE}}t_c$ of 88, 176, and 264 μs length as a function of temperature, along with fits used to extract the motional parameters listed in Table 2, and (b) Arrhenius plot of the average jump correlation times $\langle\tau_c\rangle$ as calculated from the activation parameters given in Table 2.

assuming an Arrhenius-activated average correlation time $\langle \tau_c \rangle = \tau_c^0 \exp\{E_a/RT\}$ and a temperature-independent width σ of the assumed log-normal τ_c distribution given in decades. Sample fits are shown in Figure 6a, and the fitting results are collected in Table 2 and visualized in Figure 6b. The overall fitting quality is good, with the exception of higher temperatures for the nanodisks, for which structural rearrangements, i.e., an increase of the crystallite thickness, has been reported.[13,14] It is noted that the sometimes large (~50%) error of the decay amplitude ΔM_2^{dyn} of the second moment as well as its spread in values does not exert any large influence on the fitted parameters, as it affects the average τ_c in a multiplicative way, while the variations of the latter are significant on a logarithmic scale.

The prevailing trends observed for the fitted parameters, which will be further discussed below, are (i) significantly broader τ_c distributions for the PEnd samples and (ii) on average higher activation energies for the melt-crystallized samples, coupled with the observation of unphysically low prefactors τ_c^0. Note that the activation parameters of the sample PEnd2 (see the dotted line in Figure 6b) are subject to a significantly larger fitting error. This may explain the slight deviation from the systematic trend.

B. Fast $^{13}C-^1H$ Bond Librations. Fast (<10 μs) CH bond librations in the crystalline and amorphous regions, reporting on the motional freedom related to packing and conformational constraints, are interesting in two regards. First, data for the crystallites should support the absence of contributions due to intrachain motions to the ^1H NMR data, in particular for the PEnd samples. Second, data for the amorphous regions gives a qualitative insight into the dynamics of the fold surface, as used previously to confirm differences between melt- and solution-crystallized PE.[25] It should be noted that the intracrystalline 180° jump motion is symmetry conserving for the $^{13}C-^1H$ dipolar tensor and does not have any influence on it.

Figure 7a shows a comparison of various DIPSHIFT modulation curves for the crystalline and noncrystalline regions of the samples, as distinguished by their ^{13}C chemical shift. The data are based upon the intensities of the Lorentzian functions fitted to the spectra (see Figure 4c,d), where the noncrystalline response is composed of one or two Lorentzians, depending on how many components were necessary to obtain a good fit. While the crystalline response exhibits almost no visible dependence on sample and temperature, more significant variations are seen for the noncrystalline region.

Fits using an analytical solution for CH_2 groups[59] including an exponential term accounting for the weak signal loss (apparent T_2 effect) toward $t_1 = T_{rot}$ yield the $^{13}C-^1H$ dipole–dipole coupling constants $D_{CH}/2\pi$ plotted in Figure 7b. They confirm the qualitative observations in that we find a weak yet hardly significant trend toward lower values by a few percent at higher temperature within the PE crystallites. These results are in full agreement with more quantitative ^2H NMR studies,[60] where fast librations with small 5°–12° amplitude were found between ambient temperature and 110 °C. Only the PEnd1 sample shows a somewhat more pronounced ~10% decay at the highest temperatures, which can be explained by, e.g., fast diffusion on an arc with an opening angle of 15°.[51] This slightly enhanced librational freedom may well be correlated with the slightly expanded unit cell (see Figure 3). This weak effect, and the lack of differences among the samples at temperatures below 340 K, however, confirm again that the significantly
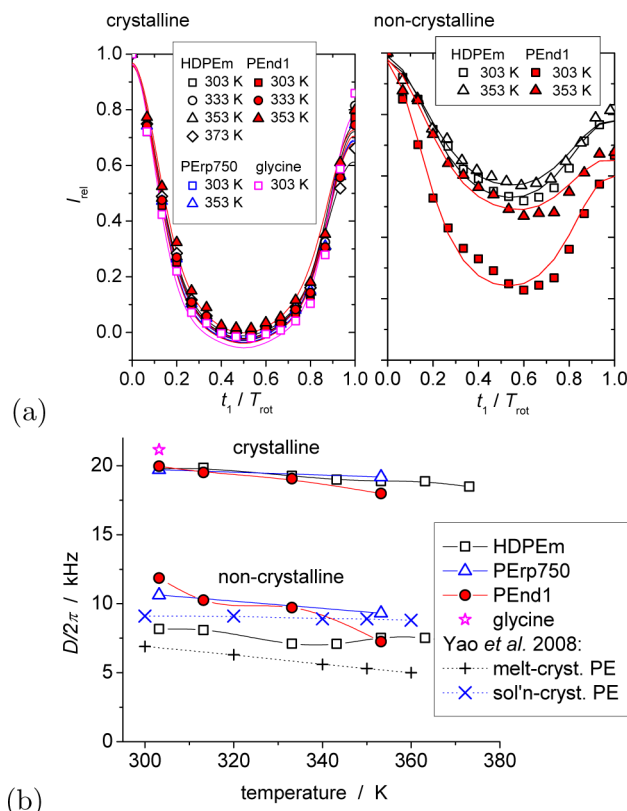

Figure 7. (a) $^{13}C-^1H$ DIPSHIFT modulation curves for different samples and temperatures for the crystalline (left panel) and the noncrystalline region (right panel) along with best-fit curves and (b) the resulting partially motion-averaged dipole–dipole coupling constants $D_{CH}/2\pi$ as a function of temperature. The glycine data provide a reference for a virtually rigid CH_2.

enhanced intracrystalline dynamics concluded from the ^1H data is not an artifact of intrachain origin.

The D_{CH} values for the noncrystalline regions vary more significantly and are in line with previous observations;[25] i.e., the PErp and PEnd samples with their tightly folded structures exhibit larger D_{CH} values than the melt-crystallized samples, confirming our assumptions on the sample morphology. The apparent T_2 effect seen in Figure 7a is somewhat stronger for the noncrystalline components and points to an influence of intermediate (μs–ms) time scale motions[61] on top of the experimental imperfections that are dominant for the crystallite signals. Notably, our D_{CH} values for PEnd1 are slightly larger than those of Yao et al. measured for solution-crystallized PE,[25] again in line with the supposition that the nanodisk samples are nearly ideal nanocrystals. The slightly larger temperature dependence observed for PEnd1 may well be due to difference in the processing of the data (component fitting vs partial integration). It should be noted that the results for the melt-crystallized samples with their larger mobile amorphous fraction are likely overestimated, as the short (0.5 ms) CP biases the spectral intensity toward the more strongly dipolar-coupled, less mobile parts closer to the crystal surface.

C. Intracrystal Chain Diffusion. Finally, we turn to an assessment of the large-scale chain transport, as detected via the exchange of ^{13}C nuclei between the initially polarized crystalline and the amorphous regions. Sample data of the decay of crystallite signal as a function of the square root of the waiting time are plotted in Figure 8a for the examples of HDPEm and
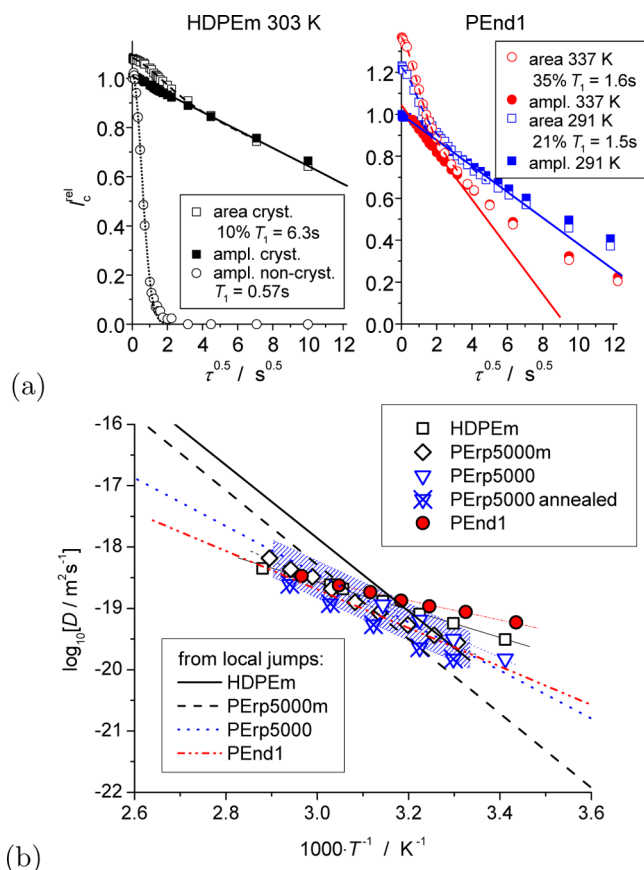
Figure 8. (a) Typical ^{13}C longitudinal magnetization decay curves for the integrals and amplitudes of the crystallite (and in one case amorphous) signal as a function of the square root of the waiting time, here measured for the HDPEm and PEnd1 samples at various temperatures along with fits (see text). (b) Arrhenius plot of the chain diffusion coefficients determined for different samples (symbols) with linear fits (thin lines) used to determine the apparent activation energies listed in Table 2. The thick lines are diffusion coefficients calculated from the local jump rates measured by ^{1}H NMR (see Figure 6 and Table 2), and the hatched area for the annealed PErp5000 sample (crossed triangles) exemplarily marks the uncertainty range as arising from uncertainties in the stem length.

PEnd1 at different temperatures. A linear initial decay in the given $\sqrt{\tau}$ representation is indicative of diffusive behavior, in line with comparably abundant data in refs 23 and 24. A detailed discussion of the dominance of diffusive behavior and possible limitations was given in ref 22.

Our data allow for a more refined critical assessment, as we find different behaviors for the crystallite signal integrals as compared to amplitudes, which are both plotted in Figure 8a so as to roughly match at intermediate times where the decay is near linear, and are jointly normalized to unity for the corresponding diffusive component. The integrals consistently reveal an additional, more quickly decaying exponential contribution of the order of 10% in most samples, which reaches higher fractions of about 25% only in the nanodisk samples at higher temperatures. This is in line with the larger dynamic heterogeneity of theses samples, as discussed above.

The additional component, for which actual exponential T_1 relaxation (with a relaxation time exceeding that of the amorphous parts) rather than diffusion appears to dominate, is clearly located in the spectral wings of the crystallite signal, as corroborated by the fact that the width of the fitted Lorentzian

decreases with increasing τ. The amplitude in turn, reflecting the center of the signal associated with well-packed stems in the lamellar core, do not show significant contributions from this component and no significant deviations from linearity. We thus assign the additional component to less well packed monomers closer to the lamellar surface, where additional fast librations of the CH_2 groups could be possible.

Fits to the integral data (shown as dashed lines in Figure 8a) assuming a sum of a single exponential and a $(1 - k\sqrt{\tau})$ decay (linear in the given representation) are consistently revealing roughly the same slope k as single-component fits to the amplitude data. This proves the inhomogeneous nature of the integrated crystallite signal and further suggests that actual T_1 contributions to the apparent diffusive decay of the dominant core fraction (peak amplitude) are weak. It should be noted that the data for the two different analysis strategies coincide beyond the plotted diffusion time range and, as compared to the initial fit, consistently reveal an upturn indicative of a distribution of diffusion coefficients rather than contributions of T_1 relaxation.

The fitted negative slope of the initial diffusive part can be related to the chain diffusion coefficient D on the basis of a one-dimensional mean-square displacement $\langle x^2 \rangle = 2D\tau$ along a stem of length s:[23,24]

$$I_c^{rel}(\tau) = \frac{I_c(\tau)}{I_c(0)} \approx 1 - \frac{\sqrt{\langle x^2 \rangle}}{s} \approx 1 - \frac{\sqrt{2D}}{d_c}\sqrt{\tau} \qquad (5)$$

$I_c(0)$ was in the plot approximated by the first available amplitude data point at $I_c(1\ ms)$, while it was a free parameter in our analyses.

In order to derive D, the stem length s must be known. We use the lamellar thickness values d_c given in Table 1 but note that this choice (or any alternative) can be quite ambiguous, as discussed below. The so-obtained chain diffusion coefficients are plotted in an Arrhenius plot (Figure 8b), where the thin lines indicate the linear fits used to extract the apparent activation energies E_a^{diff} listed in Table 2. For almost all samples we find significantly lower values as compared to the E_a characterizing the local flips, which is in line with the discrepancy also found by Yao et al.[23] However, we cannot confirm the claim of these authors that samples with a tight fold surface generally exhibit faster chain diffusion. While PEnd1 does exhibit the fastest apparent chain diffusion, the PErp samples have values well below even the melt-crystallized samples. It is also worth commenting that annealing of the PErp5000 sample at 363 K decreases the apparent D by about a factor of 5 while not changing the morphology noticeably (cf. Table 1). Thus, very subtle changes in the sample can have a large effect on the apparent large-scale chain diffusion, in agreement with similar annealing effects found by Hu et al.[19]

IV. DISCUSSION

For a critical comparison between the local jump dynamics and the large-scale chain transport, it is necessary to discuss the reliability of the different experimental approaches, which is given in this section. Figure 8b shows as thick lines diffusion coefficients calculated from the average local jump times from ^{1}H NMR (Figure 6b), based upon the related displacement of one CH_2 unit projection length. For certain temperatures, quantitative agreement is found, while the overall trends differ significantly. Notably, the variation among the samples in the high-temperature range (left-hand side of the plot) indicate

faster chain diffusion in melt-crystallized samples, whereas only little differences are inferred from the ^{13}C NMR data reflecting the chain transport. The latter data appear to merely provide a lower bound in this range. The deviations between the data from the two methods in the low-temperature range (right-hand side of the plot) are further unphysical in that ^{13}C NMR suggests faster chain diffusion than calculated based on the known local average jump time.

In order to judge the observed deviations, particular attention is to be devoted to the question whether the possible systematic errors of the experiments are sample (in)dependent. We assume that the D values obtained from ^{13}C exchange NMR are less reliable and possibly sample-dependent for a number of reasons but first discuss the validity of the ^{1}H-based approach for the characterization of the local jumps. The dipolar-echo based approach was published in ref 21. It has the advantage of reflecting the behavior of the full unbiased proton magnetization, subject to specific decay mechanisms mentioned in the Materials and Methods section. The component separation is robust within an error margin of around 5%, as reflected by the temperature variations in the crystallinities and their good correlation to results from other techniques.[21] The quantitative analysis of the crystalline response involves a correction procedure for residual dipolar dephasing, as characterized by a $T_{2,app}^{dd}(M_2)$. The variations in M_2 (see Figure 5) are not very large and never differ by more than 30% between the different samples. Further, the correction due to $T_{2,app}^{dd}$ is a factor of 3−5 weaker than the important decay due to intermediate motions which dominates $T_{2,app}$ in the relevant temperature range. This means that the M_2-related corrections do not introduce significant systematic errors; therefore, a sample-dependent bias is unlikely. The sample- and temperature-independent uncertainties in the average τ_c and the distribution width, as are apparent from the fit results (Table 2), correspond to a factor of 2 and half a decade, respectively, and cannot explain the deviations on the large τ_c scale of Figure 8b.

There is, however, a number of sample-dependent ambiguities related to the stem length (d_c) values, which enter the estimation of D from the ^{13}C-based data. First, annealing at higher temperatures, as occurring during the rather long NMR experiments, may lead to thicker lamellae. This is in fact known to be the case for the PEnd samples and has been studied in detail,[13,14] where in the studied range an increase by about 50% is possible. Similar processes may occur in the PErp samples, yet we note that we are safely below 380 K, above which a potential lamellar doubling has been reported for some specific samples.[10] Second, surface melting[62] was reported to lead to a temperature-dependent decrease of the crystallite thickness of the same order but is probably less in our samples, as concluded from the rather weakly temperature-dependent crystallinities.[21]

Third, the orientation of the chains within the crystalline lamellae is not well-known.[63,64] This issue is related to the old debate on whether a chain tilt may be a necessary condition to avoid a density anomaly in the amorphous region (see Figure 1a) for samples that are not dominated by tight folds.[65−67] The tilt angle is likely close to 35° (corresponding to a {201} fold surface) in solution-grown crystals, and very recent work has demonstrated this to be the case also for very slowly melt-crystallized HDPE.[68] Still, it may vary substantially in other samples, so for a worst-case estimate we can tentatively assume a generous uncertainty factor of 2 for the stem length (corresponding to a 60° inclination). The corresponding

results are shown in Figure 8b as the hatched area on top of the crossed triangle symbols for annealed PErp5000, which covers most of the variation range.

Fourth, any distribution effects on d_c and the actual transport process are neglected. Computer simulations[26] suggest quite a spread in d_c values and local chain mobility, at least for melt-crystallized samples. Further, our as well as Schmidt-Rohr's benchmark data[19,20] indicate a rather significant distribution of the local jump times. The effect on the initial decay can be quite strong, noting that it is dominated by the fastest fraction. This can explain the apparently larger D values from ^{13}C NMR and is supported by the finding that the apparently largest values are obtained for the PEnd1 sample with its nearly 3 decade wide distribution of jump times.

Another systematic error could arise if the small crystalline fraction dominated by actual T_1 relaxation were associated with the part of the stems closer to the fold surface (rather than to the edges of a finite nanometer-sized crystallite). This fraction increases somewhat on heating in the nanodisk samples, which means that the effective d_c value used to calculate D from signal amplitude data (reflecting the crystallite core) should be somewhat lower. Not taking this into account leads to a slight overestimation of D at higher temperatures, which, however, cannot explain too low apparent E_a^{diff} values. Finally, taking up a comment of an anonymous reviewer, it is noted that it is an open question whether for samples with tight folds a CH_2 group spends enough time in the fold region to fully relax at all temperatures investigated. This could lead to decreased apparent D values in particular at high temperatures where exchange is fast and explain a bias toward low E_a^{diff}. The clarification of this issue is beyond the scope of our work, but the fact that the reactor powders have among the largest apparent E_a^{diff} values suggests that this is not a major problem.

However, the probably most relevant source of discrepancy concerns the simplistic analysis model, eq 5. In earlier work of Schmidt-Rohr and Spiess,[22] using a similar ^{13}C-based approach probing large-scale diffusion, a more realistic model of constrained 1D diffusion was assumed, taking into account potential restrictions posed by longer and entangled loops in the amorphous regions. This accounts for a delayed signal decay toward longer τ but influences also the initial slope, in particular at high temperatures with its related larger chain displacements in a given time. This can qualitatively explain a bias of too low D values in this range and suggests another possible origin of the apparently reduced E_a^{diff} values. In fact, using the improved model, an E_a^{diff} value of 105 kJ/mol was found by Schmidt-Rohr and Spiess for a melt-crystallized sample, in very good agreement with our present and the previous values[19,20] based upon the detection of local jumps.

V. SUMMARY AND CONCLUSIONS

In summary, we have shown that a new, quantitative ^{1}H NMR approach that can be performed on a simple low-field spectrometer provides representative values for the average correlation time for local flips of the repeat units, which mediate large-scale chain diffusion in PE crystals. We have here applied the method to a comparison of intracrystal chain dynamics in different PE morphologies with ideal PE nanocrystals, and we found these to be characterized by an apparent activation energy that is significantly lower than the values of around 100 kJ/mol found for melt-crystallized samples by us and Schmidt-Rohr and co-workers.[19,20,22] This property is shared by reactor powder samples that are

characterized by a similar fold surface dominated by adjacent reentries.

The nanocrystals further feature an unusually (3 decades) wide distribution of correlation times. This finding comes along with a slightly expanded unit cell, and we attribute this to the effect of lateral pressure induced by the tight folds.[56−58] We hypothesize that the inhomogeneous chain flip rate reflects a structural inhomogeneity of the nanocrystals, which due to their small size can expand more closer to the edges and allow for faster local jumps and chain diffusion there. Reactor powders, which are characterized by larger but still highly disordered crystallites,[28] also feature a jump time distribution of 1.5−2 decades width, again significantly broader than the 1 decade wide distribution observed for melt-crystallized PE. The latter is, within our error ranges, compatible with the 0.5 decade wide distribution observed in more specialized ^{13}C-based investigations of the local jumps in melt-crystallized PE.[19]

Recent computer simulations[26] suggest that distribution effects in such samples can arise from inhomogeneities within the fold surface, where e.g. stems attached to cilia (dangling ends) were found to diffuse more quickly. Our finding of significant variability of the distribution width also settles the controversy between Schmidt-Rohr's finding of a rather narrow distribution[19] and earlier reports on the potential coexistence of fast and slow motions inferred from subtle variations in ^{13}C NMR crystalline line shapes.[69]

We were not able to confirm a recent rather general claim of much accelerated chain diffusion in PE crystals with tight fold surfaces.[23−25] The slower diffusion in other samples was explained by an additional entropic penalty and a lower "effective" jump rate, as taken from ^{13}C-based NMR experiments similar to ours, addressing large-scale chain diffusion in solution- vs melt-crystallized PE. Rather, our reactor powder samples exhibited slower chain diffusion than melt-crystallized samples, and all adjacent-reentry samples feature on average slower local jumps at high temperatures. We identified a number of ambiguities in the interpretation of such ^{13}C-based experiments, which are related to difficulties in determining the correct value for the crystalline stem length, the effect of correlation time distributions, the presence of a minor fraction of actually T_1-relaxing CH_2 units in more disordered parts of the crystallites, and constraints to free one-dimensional stem diffusion.

Early studies based upon dielectric spectroscopy[6] and Schmidt-Rohr's comparison of HDPE samples and UHMWPE fiber samples[19,20] suggest a dependence of the intracrystalline dynamics on the crystallite thickness. However, a simple and direct correlation appears unlikely in view of our data. Notably, the melt-recrystallized PErp5000m sample exhibits the thickest lamellae in the 15−20 nm range, but its intracrystalline dynamics does not deviate in a systematic way from the other samples, for which d_c is lower than 10 nm. Indirect correlations may of course exist, noting that significant variations in d_c are usually accompanied by changes in the amorphous part.

Among the remaining challenges is the identification of the molecular origin of the observed activation energy. For the adjacent-reentry type samples, we note that the E_a values in the 60−80 kJ/mol range go along with an Arrhenius prefactor τ_0 of the order of $10^{-13\pm2}$ s, which is in a realistic range of inverse frequency factors associated with molecular vibration processes. E_a could thus be explicitly related to a barrier associated with defect generation or migration. For melt-crystallized samples, the higher E_a values come with unrealistically low prefactors of

around $10^{-20\pm1}$ s. From the result plot in the previous studies on similar samples[19,20,22] we estimate similar values of about 10^{-19} and 10^{-17}–10^{-22} s, respectively. This suggests that cooperativity plays a role, for instance a coupling to Vogel−Fulcher type activation behavior in the amorphous domain, which imparts an apparent progressive slowdown, and thus a deviation from Arrhenius-type behavior, toward lower temperatures.

The question is then to explain why the local jumps are much faster in melt-crystallized samples at high temperatures (see Figure 8b), in particular in the HDPE sample with lowest molecular weight and highest polydispersity, which has the largest fraction of cilia. Noting that the NMR-detected jump rate depends on both the speed of hypothetical defect migration and their concentration, it can be speculated that the amorphous phase plays a major role. This is confirmed by the mentioned recent computer simulation study.[26] While earlier simulation work suggested major disorder and defect generation within the crystals,[7] later experimental work concluded that such significant dynamics is at variance with NMR data.[19]

Concluding, we have seen even for a polymer as well studied as PE, our knowledge on the fundamental principles behind the chain diffusion through its crystals is still limited and continues to evolve. Future fields of interest should include the study of variations in the motional freedom along the stems, crystallization from the melt vs solution, effects of branching, the influence of the molecular weight distribution, etc., details on which were outside of the scope of the present study. We envision that our results, in particular the application of our easily applicable low-field ^{1}H NMR approach to samples subjected to a wider range of thermal histories, may provide a nucleus for a more complete understanding of structure−property relationships within the important class of crystal-mobile polymers.[1]

■ AUTHOR INFORMATION

Corresponding Author
*E-mail kay.saalwaechter@physik.uni-halle.de (K.S.).

Notes
The authors declare no competing financial interest.

■ REFERENCES

(1) Hu, W.-G.; Schmidt-Rohr, K. *Acta Polym.* **1999**, *50*, 3271.
(2) Boyd, R. H. *Polymer* **1985**, *26*, 323.
(3) Ward, I. M.; Wilding, M. A. *J. Polym. Sci., Part B: Polym. Phys.* **1984**, *22*, 561.
(4) Boyd, R. H. *Polymer* **1985**, *26*, 1123.
(5) Reneker, D. H.; Fanconi, B. M.; Mazur, J. *J. Appl. Phys.* **1977**, *48*, 4032.

(6) Mansfield, M.; Boyd, R. H. *J. Polym. Sci., Part B: Polym. Phys.* **1978**, *16*, 1227.

(7) Sumpter, B. G.; Noid, D. W.; Wunderlich, B. *Macromolecules* **1992**, *25*, 7247.

(8) Till, P. H. *J. Polym. Sci.* **1957**, *24*, 301.

(9) Organ, S. J.; Keller, A. *J. Mater. Sci.* **1985**, *20*, 1571.

(10) Rastogi, S.; Spoelstra, A. B.; Goossens, J. G. P.; Lemstra, P. J. *Macromolecules* **1997**, *30*, 7880.

(11) Keller, A.; Hikosaka, M.; Rastogi, S.; Toda, A.; Barham, P. J.; Goldbeck-Wood, G. *J. Mater. Sci.* **1994**, *29*, 2579.

(12) Weber, C. H. M.; Chiche, A.; Krausch, G.; Rosenfeldt, S.; Ballauff, M.; Harnau, L.; Gottker-Schnetmann, I.; Tong, Q.; Mecking, S. *Nano Lett.* **2007**, *7*, 2024.

(13) Rochette, C. N.; Rosenfeldt, S.; Henzler, K.; Polzer, F.; Ballauff, M.; Tong, Q.; Mecking, S.; Drechsler, M.; Narayanan, T.; Harnau, L. *Macromolecules* **2011**, *44*, 4845.

(14) Osichow, A.; Rabe, C.; Vogtt, K.; Narayanan, T.; Harnau, L.; Drechsler, M.; Ballauff, M.; Mecking, S. *J. Am. Chem. Soc.* **2013**, *153*, 11645.

(15) Pandey, A.; Champouret, Y.; Rastogi, S. *Macromolecules* **2011**, *44*, 4952.

(16) Schmidt-Rohr, K.; Spiess, H. W. *Multidimensional Solid-State NMR and Polymers*; Academic Press: London, 1994.

(17) Levitt, M. H. *Spin Dynamics*; Wiley: London, 2001.

(18) Duer, M. J., Ed.; *Solid-State NMR Spectroscopy: Principles and Applications*; Blackwell Science Ltd.: Oxford, 2002.

(19) Hu, W.-G.; Boeffel, C.; Schmidt-Rohr, K. *Macromolecules* **1999**, *32*, 1611.

(20) Hu, W.-G.; Boeffel, C.; Schmidt-Rohr, K. *Macromolecules* **1999**, *32*, 1714.

(21) Bärenwald, R.; Champouret, Y.; Saalwächter, K.; Schäler, K. *J. Phys. Chem. B* **2012**, *116*, 13089.

(22) Schmidt-Rohr, K.; Spiess, H. W. *Macromolecules* **1991**, *24*, 5288.

(23) Yao, Y. F.; Graf, R.; Spiess, H. W.; Lippits, D. R.; Rastogi, S. *Phys. Rev. E* **2007**, *76*, 060801(R).

(24) Yao, Y.; Graf, R.; Spiess, H. W.; Rastog, S. *Macromol. Rapid Commun.* **2009**, *30*, 1123.

(25) Yao, Y. F.; Graf, R.; Spiess, H. W.; Rastogi, S. *Macromolecules* **2008**, *41*, 2514.

(26) Yamamoto, T. *Macromolecules* **2010**, *43*, 9384.

(27) Göttker-Schnetmann, I.; Korthals, B.; Mecking, S. *J. Am. Chem. Soc.* **2006**, *128*, 7708.

(28) Egorov, V. M.; Ivan'kova, E. M.; Marikhin, V. A.; Myasnikova, L. P. *J. Macromol. Sci., Phys.* **2002**, *B41*, 939.

(29) VanderHart, D. L.; Khoury, F. *Polymer* **1984**, *25*, 1589.

(30) Röthemeyer, F.; Sommer, F. *Kautschuktechnologie*; Carl Hanser Verlag: München, 2006.

(31) Michler, G. H.; Naumann, I. *Acta Polym.* **1982**, *33*, 399.

(32) Michler, G. H. *Electron Microscopy of Polymers*; Springer-Verlag: Berlin, 2008.

(33) Bunn, C. W. *Trans. Faraday Soc.* **1939**, *35*, 482.

(34) Matsui, S. *Chem. Phys. Lett.* **1991**, *179*, 187.

(35) Rhim, W.-K.; Pines, A.; Waugh, J. S. *Phys. Rev. B* **1971**, *3*, 684.

(36) Hansen, E. W.; Kristiansen, P. E.; Pedersen, B. *J. Phys. Chem. B* **1998**, *102*, 5444.

(37) Hedesiu, C.; Demco, D. E.; Kleppinger, R; Buda, A. A.; Blümich, B.; Remerie, K.; Litvinov, V. M. *Polymer* **2007**, *48*, 763.

(38) Bergmann, K. *J. Polym. Sci., Part B: Polym. Phys.* **1978**, *16*, 1661.

(39) Mandelkern, L.; Alamo, R. G.; Kennedy, M. *Macromolecules* **1990**, *23*, 4721.

(40) Cheng, J.; Fone, M.; Reddy, V. N.; Schwartz, K. B.; Fisher, H. P.; Wunderlich, B. *J. Polym. Sci., Part B: Polym. Phys.* **1994**, *32*, 2683.

(41) Olf, H. G.; Peterlin, A. *Kolloid Z. Z. Polym.* **1967**, *215*, 97.

(42) Olf, H. G.; Peterlin, A. *J. Polym. Sci., Part A-2* **1970**, *8*, 771.

(43) Anderson, P. W.; Weiss, P. R. *Rev. Mod. Phys.* **1953**, *25*, 269.

(44) Fechete, R.; Demco, D. E.; Blümich, B. *J. Chem. Phys.* **2003**, *118*, 2411.

(45) Sturniolo, S.; Saalwächter, K. *Chem. Phys. Lett.* **2011**, *516*, 106.

(46) Demco, D. E.; Johansson, A.; Tegenfeldt, J. *Solid State Nucl. Magn. Reson.* **1995**, *4*, 13.

(47) Fung, B. M.; Khitrin, A. K.; Ermolaev, K. *J. Magn. Reson.* **2000**, *142*, 97.

(48) Earl, W. L.; VanderHart, D. L. *Macromolecules* **1979**, *12*, 762.

(49) Tonelli, A. E. *NMR Spectroscopy and Polymer Microstructure: The Conformational Connection*; VCH: Weinheim, 1989.

(50) Munowitz, M.; Griffin, R. G.; Bodenhausen, G.; Huang, T. H. *J. Am. Chem. Soc.* **1981**, *103*, 2529.

(51) Reichert, D.; Saalwächter, K. In *NMR Crystallography (Encyc. Magn. Reson.)*; Harris, R. K., Wasylishen, R. E., Duer, M. J., Eds.; John Wiley & Sons: Chichester, 2009; pp 177−193.

(52) Schäler, K.; Achilles, A.; Bärenwald, R.; Hackel, C.; Saalwächter, K. *Macromolecules* **2013**, *46*, 7818.

(53) Kurz, R.; Cobo, M. F.; Sommer, E. R. d. M.; Wicklein, A.; Thelakkat, M.; Hempel, G.; Saalwächter, K. *ChemPhysChem* **2013**, *14*, 3146.

(54) Kitamaru, R.; Horii, F.; Murayama, K. *Macromolecules* **1986**, *19*, 636.

(55) Torchia, D. A. *J. Magn. Reson.* **1978**, *30*, 613.

(56) Rault, J. *J. Macromol. Sci., Phys. B* **1976**, *12*, 335.

(57) Cammarata, R.; Eby, R. *J. Mater. Res.* **1991**, *6*, 888.

(58) Hütter, M.; in't Veld, P. J.; Rutledge, G. C. *Polymer* **2006**, *47*, 5494.

(59) Hackel, C.; Zinkevich, T.; Belton, P.; Achilles, A.; Reichert, D.; Krushelnitsky, A. *Phys. Chem. Chem. Phys.* **2012**, *14*, 2727.

(60) Hentschel, D.; Sillescu, H.; Spiess, H. W. *Makromol. Chem.* **1979**, *180*, 241.

(61) deAzevedo, E. R.; Saalwächter, K.; Pascui, O.; de Souza, A. A.; Bonagamba, T. J.; Reichert, D. *J. Chem. Phys.* **2008**, *128*, 104505.

(62) Albrecht, T.; Strobl, G. *Macromolecules* **1995**, *28*, 5827.

(63) Gautam, S.; Balijepalli, S.; Rutledge, G. C. *Macromolecules* **2000**, *33*, 9136.

(64) Gedde, U. W.; Mattozzi, A. *Adv. Polym. Sci.* **2004**, *169*, 29.

(65) Frank, F. C. *Faraday Discuss.* **1979**, *68*, 7.

(66) Hoffman, J. D.; Guttman, C. M.; DiMarzio, E. A. *Faraday Discuss.* **1979**, *68*, 177.

(67) Yoon, D. Y.; Flory, P. J. *Macromolecules* **1984**, *17*, 868.

(68) Rosenthal, M.; Bar, G.; Burghammer, M.; Ivanov, D. A. *Angew. Chem., Int. Ed.* **2011**, *50*, 8881.

(69) Hillebrand, L.; Schmidt, A.; Bolz, A.; Hess, M.; Veeman, W.; Meier, R. J.; van der Velden, G. *Macromolecules* **1998**, *31*, 5010.